

Radio Emission Reveals Inner Meter-Scale Structure of Negative Lightning Leader Steps

B. M. Hare^{1,2,*}, O. Scholten^{1,2,3,†}, J. Dwyer,⁴ U. Ebert^{5,6}, S. Nijdam⁶, A. Bonardi,⁷ S. Buitink,^{7,8} A. Corstanje,^{7,8} H. Falcke,^{7,9,10,11} T. Huege,^{8,12} J. R. Hörandel,^{7,8,9} G. K. Krampah⁸, P. Mitra,⁸ K. Mulrey,⁸ B. Neijzen,¹ A. Nelles,^{13,14} H. Pandya⁸, J. P. Rachen,⁸ L. Rossetto,⁷ T. N. G. Trinh¹⁵, S. ter Veen,¹⁰ and T. Winchen⁸

¹University of Groningen, KVI Center for Advanced Radiation Technology, 9747 AA Groningen, Netherlands

²University of Groningen, Kapteyn Astronomical Institute, Groningen 9700 AV, Netherlands

³Interuniversity Institute for High-Energy, Vrije Universiteit Brussel, Pleinlaan 2, 1050 Brussels, Belgium

⁴Department of Physics and Space Science Center (EOS), University of New Hampshire, Durham, New Hampshire 03824, USA

⁵CWI, Centrum Wiskunde & Informatica, 1098 XG Amsterdam, Netherlands

⁶TU/e, Eindhoven University of Technology, 5612 AZ Eindhoven, Netherlands

⁷Department of Astrophysics/IMAPP, Radboud University Nijmegen, 6525 XZ Nijmegen, Netherlands

⁸Astrophysical Institute, Vrije Universiteit Brussel, Pleinlaan 2, 1050 Brussels, Belgium

⁹Nikhef, Science Park Amsterdam, 1098 XG Amsterdam, Netherlands

¹⁰Netherlands Institute for Radio Astronomy (ASTRON), 7991 PD Dwingeloo, Netherlands

¹¹Max-Planck-Institut für Radioastronomie, 53121 Bonn, Germany

¹²Institut für Kernphysik, Karlsruhe Institute of Technology(KIT), P.O. Box 3640, 76021, Karlsruhe, Germany

¹³Erlangen Center for Astroparticle Physics, Friedrich-Alexander-Universität Erlangen-Nürnberg, 91058, Erlangen, Germany

¹⁴DESY, Platanenallee 6, 15738, Zeuthen, Germany

¹⁵Department of Physics, School of Education, Can Tho University Campus II, 3/2 Street, Ninh Kieu District, Can Tho City, Vietnam

(Received 27 August 2019; revised manuscript received 29 November 2019; accepted 6 February 2020; published 10 March 2020)

We use the Low Frequency Array (LOFAR) to probe the dynamics of the stepping process of negatively charged plasma channels (negative leaders) in a lightning discharge. We observe that at each step of a leader, multiple pulses of vhf (30–80 MHz) radiation are emitted in short-duration bursts ($< 10 \mu\text{s}$). This is evidence for streamer formation during corona flashes that occur with each leader step, which has not been observed before in natural lightning and it could help explain x-ray emission from lightning leaders, as x rays from laboratory leaders tend to be associated with corona flashes. Surprisingly, we find that the stepping length is very similar to what was observed near the ground, however with a stepping time that is considerably larger, which as yet is not understood. These results will help to improve lightning propagation models, and eventually lightning protection models.

DOI: [10.1103/PhysRevLett.124.105101](https://doi.org/10.1103/PhysRevLett.124.105101)

Lightning is one of the most energetic processes in our atmosphere. It is thought to initiate from a single point, that then separates into positively and negatively charged ends, called positive and negative leaders, which propagate away from the initiation point and into oppositely charged cloud regions [1]. At the tip of each leader many streamer discharges create weakly ionized plasma channels through the joint action of ionization fronts and local field enhancement at the front of the streamer channels. For positive leaders, electrons accelerate toward the leader, allowing the positive leader to grow fairly gradually while supported by the strong photoionization in air as a source of free electrons [2–4]. We have recently developed new high-resolution vhf measurement techniques and applied them to positive leaders [5].

In this work we focus on negative leaders. Negative leaders have a significantly more complex propagation mechanism where they propagate in discrete steps. Each step appears to be due to luminous structures, generally assumed to be conducting (see Ref. [6] for an alternative

interpretation) that form in front of the main conducting channel, called space stems in this work. After their formation, these structures grow backward to connect with the main leader body, resulting in a large current pulse to equalize the electric potential. This process was first observed in laboratory discharges [2,7] and later in lightning [8–10]. However, the majority of the previous work has been done in the optical regime, which does not directly relate to electrical current (see, e.g., Ref. [6]), or using radio emission below 10 MHz that is only sensitive to larger scale electrical currents (see, e.g., Refs. [11,12]). The stepping process has been observed before in vhf emission [13], however with a resolution that made it difficult to draw firm conclusions.

To investigate the mechanism behind negative leader propagation and its vhf emission we have used the LOFAR to provide measurements of the meter-scale distribution of electrical currents in negative leaders using the technique described in Ref. [5]. These measurements will help to improve lightning leader

modeling, which tends to rely on a large number of assumptions, inhibiting, for example, our understanding of basic lightning processes such as attachment to ground, which is critical for improved lightning protection [14,15]. Furthermore, previous work has shown that the majority of terrestrial gamma-ray flashes, intense bursts of gamma-ray radiation with energies up to 10 MeV, are correlated with negative leader stepping [1]; therefore, our improved understanding of leader propagation could be used in future work to help understand terrestrial gamma-ray flashes.

We show that each leader step emits a burst of multiple discrete vhf pulses. This is in direct contrast with what is expected based on previous work, which predicts one single vhf source per step [12]. We find that the majority of vhf sources in a leader step occur within about a meter of each other, showing that vhf radiation from negative leaders comes from corona flashes, which have been observed in laboratory sparks but not in natural lightning [16,17]. This discovery could explain why lightning leaders tend to emit 100–500 keV x rays, since similar x-ray bursts seen in laboratory sparks are often associated with corona flashes [16,18].

LOFAR is a distributed radio telescope that is primarily built for radio-astronomy observations [19] but has also proven to be an excellent cosmic-ray air-shower detector [20,21]. Its potential for lightning detection was clear at the initial design [22]. We use the Dutch part of LOFAR consisting of thousands of dipole antennas spread over 3200 km² in northern Netherlands with antennas operating in the 30–80 MHz band. The traces are sampled at 200 MHz and the relative arrival time of each pulse can be measured with about 1 ns accuracy. Our algorithm can locate sources that are at least 120 ns apart.

Previous techniques could map lightning in either 3D with about 100 m accuracy [23] or in 2D with 1° accuracy [24]. Our technique allows us to map lightning in 3D with a horizontal accuracy better than 2 and 15 m vertically with an efficiency of one source per 1 μs [5].

We analyze a lightning flash from September 29, 2017 [5], where the discharge initiated at a height of 4 km. Over time, extended structures are formed with several positive and negative leaders spanning distances of 5 km. In Ref. [5] we focused on the structure of the positive leaders in this flash, and here we analyze the negative ones. Each located source has an interferometric fit value that lies between 0 and 1, where 1 is the best possible fit. In order to achieve a horizontal location accuracy of 1 m, we only used sources that had an interferometric fit value larger than 0.87 while in Ref. [5] we used sources with fit values larger than 0.85, which resulted in a horizontal location accuracy around 2 m. Our new criterion of 0.87 removes 16% of the sources that were shown in Ref. [5]. The qualitative results of this study would not change if we used the lower cut of 0.85 instead of 0.87.

Negative leaders easily extend over distances of several kilometers. The LOFAR measurements allow us to zoom in

on a small section of such a negative leader spanning only 100 m as shown in Fig. 1. Each dot corresponds to the position of a source emitting a single vhf pulse. The location has been determined from the detected arrival time of the pulse at each LOFAR antenna. Each vhf pulse has a full width at half maximum of about 50 ns, which is mostly dominated by LOFAR’s antenna pulse response. We find that these radio sources on negative leaders come in bursts. These bursts can be seen in Fig. 1, where the vhf sources tend to cluster in time. A wider view of this leader is shown in the Supplemental Material [25]. These bursts are observed across all well-imaged negative leaders. The obvious interpretation is that these bursts are due to leader stepping.

Figure 2 shows a distribution of time between subsequent radio sources across 26 negative leader segments, with a total length of about 15 km, in the 2017 lightning flash. If every radio source were randomly distributed in time, the time between radio sources would be exponentially distributed. The distribution strongly deviates from an exponential; in particular, there is a sharp spike below time differences of 4 μs that shows that our located sources cluster together in time significantly more than could be possible for random chance. This spike continues down to 120 ns, the smallest time differences that can be probed with our present imaging algorithm.

It is ambiguous how to precisely define which sources should be clustered together in a burst. This is expressed by

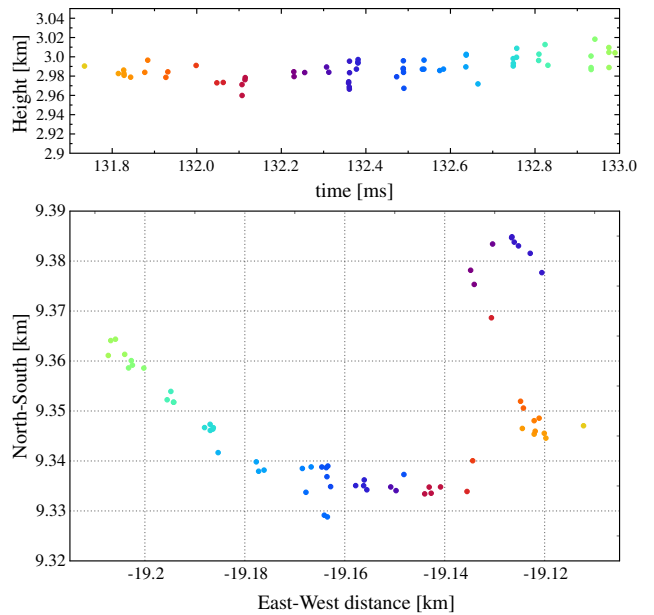


FIG. 1. A section of a negative leader where each dot is the location of a reconstructed source. Top: Height versus emission time of the source. Bottom: Projection of the source position on the ground plane where distances are measured from the core of LOFAR. The color of each dot reflects emission time going from yellow to green.

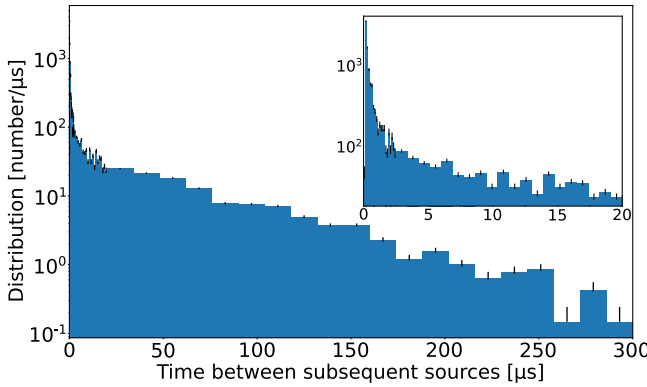


FIG. 2. The distribution of time between subsequent sources. The error bars show the lowest and largest Poisson rates that can model the data with 34% confidence (1σ).

the fact that the distribution in Fig. 2 is very smooth. In lieu of a physics-inspired definition, we have defined a burst such that every located source in a burst is within $2 \mu\text{s}$ of its subsequent radio source. This time cut was chosen because (1) it includes the majority of vhf sources shown in the spike in Fig. 2, (2) it is short enough that it minimizes the chance of vhf sources from different leader steps to interfere with our results, and (3) the qualitative results are similar even if the time is halved or doubled. The number of sources in a burst may thus vary from a single one up to a maximum of 9 located sources, using this prescription. Of the total of 2599 bursts, we have 224 bursts with 3 or more sources. Investigation of the vhf time traces shows that the majority of bursts with a single located source even have multiple vhf pulses that are not located but most probably come from the same spot. If we use instead $8 \mu\text{s}$ in the definition of a burst we obtain qualitatively very similar numbers (2204 bursts of which 340 have 3 or more sources). We find that the strength of the pulses within a burst varies greatly; in addition, some burst may contain three strong pulses while others may have a single much weaker one.

Figure 3 shows the spatial distribution of sources within a burst that have three or more located sources by binning the horizontal distance between each source and the geometric center of all pulses in the burst. Note that we focus on the horizontal plane, since our horizontal location accuracy (around 1 m) is significantly better than our vertical location accuracy (around 10 m). Also shown is a simulated distribution if every radio source in a burst came from the same location with a location error of 1 m. The fact that 2/3 of the data-derived distribution is within the radius of our simulation shows that our data are consistent with the majority of located sources in a burst coming from the same location. This can also be seen from Fig. 1, where the different bursts in the time versus height plot are also localized after projecting on the ground plane. However, there are also many bursts where the sources are spread

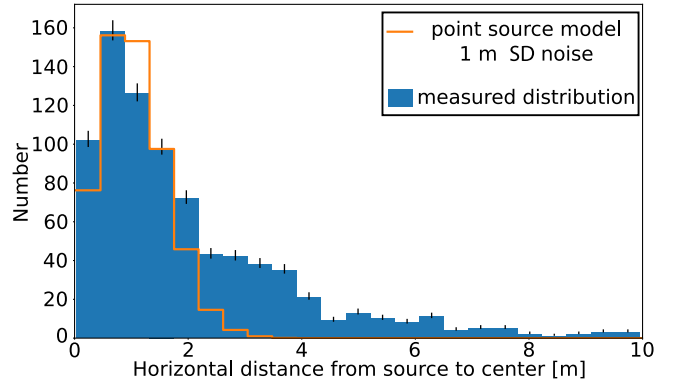


FIG. 3. The histogram shows the horizontal spatial distribution of pulses in bursts. The orange line gives the simulation results if the sources are at one location with a 1 m horizontal location accuracy and accounts for 2/3 of the number of sources. The error bars indicate the lowest and highest Poisson rates that could model the data within 34% confidence (1σ).

over larger distances. This is expressed by the shoulder in the distribution at a distance of 3.5 m. This shoulder persists independent of changes in our quality cut, burst definition, or specific set of leaders used in the analysis. Bursts with spatial extent seem to be mostly due to simultaneous activity in close branches, and due to bursts that are extended lengthwise along the channel (with lengths around 5 m). The Supplemental Material includes figures that show a variety of different bursts [25].

The total duration of a burst (for bursts with at least 2 pulses) is exponentially distributed with a median of $0.5 \mu\text{s}$ and a suppression below $0.1 \mu\text{s}$. Changing our burst definition to $8 \mu\text{s}$ increases the median considerably to $1.5 \mu\text{s}$ by adding a long tail extending to $4 \mu\text{s}$. Even though the density of located sources in the flash is second to none, it should be realized that our imaging formalism has an efficiency of only 30%; i.e., only a third of the strongest pulses in a spectrum are located. This probably most strongly affects the burst duration. For example, if a pulse in the middle of a burst is not imaged, then our simple $2 \mu\text{s}$ definition may split that burst in two, while a $8 \mu\text{s}$ definition may combine multiple bursts.

The time distribution between bursts shows an exponential distribution, see Fig. 4, with a median at $40 \mu\text{s}$ which we interpret as the median stepping time. This number is not affected much by the precise definition of a burst since using the $8 \mu\text{s}$ burst definition yields a median stepping time of $50 \mu\text{s}$. The horizontal distance between bursts also shows an exponential distribution with a cutoff at distances below 4 m and a median of 7.5 m where the median shifts to 8.5 m for the $8 \mu\text{s}$ burst definition. We have taken here the distance as measured in the horizontal plane because our vertical resolution is of the order of 10 m and thus would confuse the picture. Optical observations of leader growth well below the cloud have found that the time between negative leader steps tends to be around $10 \mu\text{s}$ and

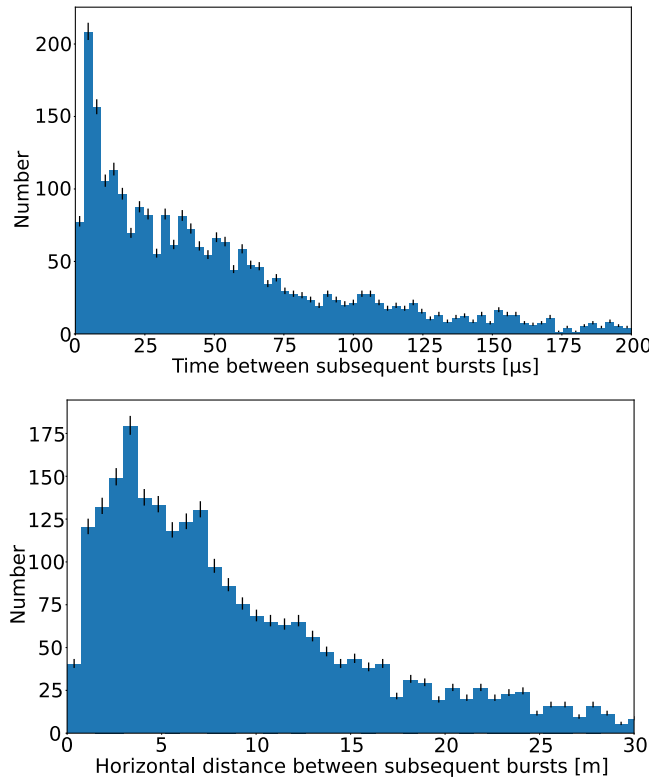


FIG. 4. Time between bursts (top) and horizontal distance between bursts (bottom), where a burst can have only a single pulse.

their length tends to be around 5 m [8]. We thus observe that in the cloud the stepping time is considerably longer than close to ground with a stepping length that is only marginally larger. Near ground level one could expect stronger electric fields than in a cloud, but how this reflects in the observed differences is not understood.

A very common interpretation of the negative leader stepping process is that when the space stem connects to the existing leader, there is a current pulse that equalizes the voltage in the space stem to the much larger (negative) voltage at the tip of the leader by removing positive charge from the space stem [12]. In the process, the space stem, which was poorly conducting, heats up due to the dissipation of the electric energy of the current, ionizes further, and becomes a good conducting heated plasma, thus forming a new leader section. This sudden voltage jump will cause the electric field to exceed breakdown ($E_c = 3.2 \text{ MV/m}$ in air at STP) and produce an inception cloud, where a semispherical ionization front expands until the electric field on its surface drops to the breakdown value. Subsequently this ionization front breaks up into many streamers [17,26], thin channels of ionized air that grow due to the field enhancement and ionization fronts at their tips. The process of suddenly forming a multitude of streamers during a leader step is also known as a corona flash [27,28]. The streamers will then, somehow, generate a new space stem that will then grow backward toward the

leader, allowing the whole process to repeat. It is thought that a space stem is formed from merging streamers, but the process is not understood. An alternative theory was recently suggested in Ref. [6].

One could imagine that the radio emission is due to the large current pulse at the time when the space stem connects to the main leader channel; however, this simple model is not consistent with our data since it predicts a single pulse at each leader step while we observe a whole burst of pulses. This single pulse is, however, regularly observed below 10 MHz [9,11]. In Ref. [29] a model is proposed where vhf emission is generated by collisions between streamers, but it is not clear how to compare this model to our data.

A likely mechanism for the emission of pulses in bursts is the process where the inception cloud breaks up into a multitude of streamers [30], much like has been observed in laboratory experiments [17,26,30]. This fits our observation in Fig. 3 that the dominating emission is nearly point-source-like at the tip of the leader, with a few sources coming from a short distance ($\approx 3.5 \text{ m}$) along the body of the leader. Note that positive leaders in the laboratory, often do not exhibit corona flashes, which could explain why negative leaders emit significantly more vhf radiation than positive leaders [31].

Based on the amplitude of the pulses we observe, we infer that energy emitted by the strongest radio source regions that we receive has an order of magnitude of $4 \times 10^{-6} \text{ J}$ in our 30–80 MHz frequency band. This roughly equates to a streamer with an order of magnitude of 5×10^{13} free electrons. Details of these order-of-magnitude calculations are given in Supplemental Material [25], which includes Refs. [32–36]. This is consistent with the idea that there are of the order of 10^5 streamers [18] in a corona flash, distributed in strength of emitted vhf energy, where we are only sensitive to the extreme tail of that distribution. Future work is needed to find the distribution of detected streamer sizes.

As mentioned before, the large current pulse during a step moves the negative charge cloud over the length of the step. The radio emission during this step must have a wavelength of at least the spatial extent of the charge cloud (expected to be tens of meters) to be coherent and thus strong. Thus, the radiation from the stepping current itself has a peak intensity at frequencies well below the LOFAR band of 30–80 MHz (10–3.8 m wavelength), which would explain why this signal is not clearly visible in our data. It therefore would be very interesting to perform simultaneous measurements in the 100 kHz–10 MHz band, where such current pulses are regularly observed.

In this work we have established that the vhf emission seen from stepping negative leaders in lightning is most likely due to streamer formation around the region of the step. The vhf emission appears concentrated near the tip of the leader, potentially where the inception cloud breaks up

into streamers during a corona flash, which has not been observed in natural lightning before. There is also emission along the body of the step, potentially due to spurious streamer emission from the body of the leader.

The LOFAR cosmic-ray key science project acknowledges funding from an Advanced Grant of the European Research Council (FP/2007-2013), ERC Grant Agreement No. 227610. The project has also received funding from the European Research Council (ERC) under the European Union's Horizon 2020 research and innovation programme (Grant Agreement No. 640130). We furthermore acknowledge financial support from FOM (FOM-Project No. 12PR304). A.N. is supported by the DFG (NE 2031/2-1). T.W. is supported by DFG Grant No. 4946/1-1. This Letter is based on data obtained with the International LOFAR Telescope (ILT). LOFAR [19] is the Low Frequency Array designed and constructed by ASTRON. It has observing, data processing, and data storage facilities in several countries, that are owned by various parties (each with their own funding sources), and that are collectively operated by the ILT foundation under a joint scientific policy. The ILT resources have benefitted from the following recent major funding sources: CNRS-INSU, Observatoire de Paris and Université d'Orléans (France); BMBF, MIWF-NRW, MPG (Germany); Science Foundation Ireland (SFI), Department of Business, Enterprise and Innovation (DBEI) (Ireland); NWO (Netherlands); The Science and Technology Facilities Council (United Kingdom).

*B.H.Hare@rug.nl

[†]O.Scholten@rug.nl

- [1] J. R. Dwyer and M. A. Uman, *Phys. Rep.* **534**, 147 (2014).
- [2] I. Gallimberti, G. Bacchigia, A. Bondiou-Clergerie, and P. Lalande, *C. R. Phys.* **3**, 1335 (2002).
- [3] G. Wormeester, S. Pancheshnyi, A. Luque, S. Nijdam, and U. Ebert, *J. Phys. D* **43**, 505201 (2010).
- [4] C. J. Biagi, M. A. Uman, J. D. Hill, and D. M. Jordan, *Geophys. Res. Lett.* **38**, L24809 (2011).
- [5] B. Hare *et al.*, *Nature (London)* **568**, 360 (2019).
- [6] A. Malagón-Romero and A. Luque, *Geophys. Res. Lett.* **46**, 4029 (2019).
- [7] Les Renardières Group, *Electra* **74**, 67 (1981).
- [8] J. D. Hill, M. A. Uman, and D. M. Jordan, *J. Geophys. Res.* **116**, D16117 (2011).
- [9] C. J. Biagi, M. A. Uman, J. D. Hill, and D. M. Jordan, *J. Geophys. Res.* **119**, 8160 (2014).
- [10] W. R. Gamerota, M. A. Uman, J. D. Hill, and D. M. Jordan, *Geophys. Res. Lett.* **42**, 1977 (2015).
- [11] J. Howard, M. A. Uman, C. Biagi, D. Hill, V. A. Rakov, and D. M. Jordan, *J. Geophys. Res.* **116**, D08201 (2011).
- [12] B. E. Carlson, C. Liang, P. Bitzer, and H. Christian, *J. Geophys. Res.* **120**, 5316 (2015).

- [13] W. P. Winn, G. D. Aulich, S. J. Hunyady, K. B. Eack, H. E. Edens, P. R. Krehbiel, W. Rison, and R. G. Sonnenfeld, *J. Geophys. Res.* **116**, D23115 (2011).
- [14] Special Issue Dedicated to the 30th International Conference on Lightning Protection (ICLP), edited by V. Cooray and M. Becerra [*Atmos. Res.* **117**, 64 (2012)].
- [15] V. Cooray and L. Arevalo, *Atmosphere-Ocean* **8**, 245 (2017).
- [16] P. O. Kochkin, A. P. J. van Deursen, and U. Ebert, *J. Phys. D* **48**, 025205 (2015).
- [17] A. Y. Kostinskiy, V. S. Syssoev, N. A. Bogatov, E. A. Mareev, M. G. Andreev, M. U. Bulatov, D. I. Sukharevsky, and V. A. Rakov, *J. Geophys. Res.* **123**, 5360 (2018).
- [18] S. Celestin, W. Xu, and V. P. Pasko, *J. Geophys. Res.* **120**, 10712 (2015).
- [19] M. P. van Haarlem *et al.*, *Astron. Astrophys.* **556**, A2 (2013).
- [20] H. Falcke *et al.*, *Nature (London)* **435**, 313 (2005).
- [21] S. Buitink *et al.*, *Nature (London)* **531**, 70 (2016).
- [22] I. Holleman, H. Beekhuis, S. Noteboom, L. G. Evers, H. Haak, and H. Falcke, in *Proceedings of the International Lightning Detection Conference (ILDC 2006)*, Tucson, AZ, <https://my.vaisala.net/en/events/ldcilmc/archive/Pages/ILDC-2006-Archive.aspx>.
- [23] W. Rison, R. J. Thomas, P. R. Krehbiel, T. Hamlin, and J. Harlin, *Geophys. Res. Lett.* **26**, 3573 (1999).
- [24] M. G. Stock, M. Akita, P. R. Krehbiel, W. Rison, H. E. Edens, Z. Kawasaki, and M. A. Stanley, *J. Geophys. Res.* **119**, 3134 (2014).
- [25] See Supplemental Material at <http://link.aps.org/supplemental/10.1103/PhysRevLett.124.105101> for estimation of emitted source power and more figures of bursts.
- [26] S. Chen, L. C. J. Heijmans, R. Zeng, S. Nijdam, and U. Ebert, *J. Phys. D* **48**, 175201 (2015).
- [27] E. M. Bazelyan and Y. P. Raizer, in *Lightning Physics and Lightning Protection* (IOP Publications, Bristol, 2000), p. 199, <https://epdf.pub/lightning-physics-and-lightning-protection.html>.
- [28] P. Kochkin, A. van Deursen, and U. Ebert, *J. Phys. D* **47**, 145203 (2014).
- [29] F. Shi, N. Liu, J. R. Dwyer, and K. M. A. Ihaddadene, *Geophys. Res. Lett.* **46**, 443 (2019).
- [30] T. M. P. Briels, E. M. van Veldhuizen, and U. Ebert, *IEEE Trans. Plasma Sci.* **36**, 908 (2008).
- [31] P. Kochkin, C. Nguyen, A. van Deursen, and U. Ebert, *J. Phys. D* **45**, 425202 (2012).
- [32] B. Neijzen, Negative leader propagation, Bachelor's thesis, FSE, KVI-CART, University of Groningen, 2019, <http://fse.studenttheses.ub.rug.nl/19915/>.
- [33] K. Mulrey, A. Bonardi, S. Buitink, A. Corstanje, H. Falcke, B. Hare, J. Hörandel, T. Huege, P. Mitra, A. Nelles, J. Rachen, L. Rossetto, P. Schellart, O. Scholten, S. ter Veen, S. Thoudam, T. Trinh, and T. Winchen, *Astropart. Phys.* **111**, 1 (2019).
- [34] J. Qin and V. P. Pasko, *J. Phys. D* **47**, 435202 (2014).
- [35] T. Briels, J. Kos, E. Veldhuizen, and U. Ebert, *J. Phys. D* **39**, 5201 (2006).
- [36] A. Luque and U. Ebert, *New J. Phys.* **16**, 013039 (2014).

Radio emission from negative lightning leader steps reveals inner meter-scale structure: Supplementary Material

B. M. Hare,^{1,*} O. Scholten,^{1,2,†} J. Dwyer,³ U. Ebert,^{4,5} S. Nijdam,⁵ A. Bonardi,⁶ S. Buitink,^{6,7} A. Corstanje,^{6,7} H. Falcke,^{6,8,9,10} T. Huege,^{7,11} J. R. Hörandel,^{6,7,8} G. K. Krampah,⁷ P. Mitra,⁷ K. Mulrey,⁷ B. Neijzen,¹ A. Nelles,^{12,13} H. Pandya,⁷ J. P. Rachen,⁷ L. Rossetto,⁶ T. N. G. Trinh,¹⁴ S. ter Veen,⁹ and T. Winchen⁷

¹ University of Groningen, KVI Center for Advanced Radiation Technology, Groningen, The Netherlands

² Interuniversity Institute for High-Energy, Vrije Universiteit Brussel, Pleinlaan 2, 1050 Brussels, Belgium

³ Department of Physics and Space Science Center (EOS), University of New Hampshire, Durham NH 03824 USA

⁴ CWI, Centrum Wiskunde & Informatica, Amsterdam, The Netherlands

⁵ TU/e, Eindhoven University of Technology, Eindhoven, The Netherlands

⁶ Department of Astrophysics/IMAPP, Radboud University Nijmegen, Nijmegen, The Netherlands

⁷ Astrophysical Institute, Vrije Universiteit Brussel, Pleinlaan 2, 1050 Brussels, Belgium

⁸ Nikhef, Science Park Amsterdam, Amsterdam, The Netherlands

⁹ Netherlands Institute for Radio Astronomy (ASTRON), Dwingeloo, The Netherlands

¹⁰ Max-Planck-Institut für Radioastronomie, Bonn, Germany

¹¹ Institut für Kernphysik, Karlsruhe Institute of Technology(KIT), P.O. Box 3640, 76021, Karlsruhe, Germany

¹² Erlangen Center for Astroparticle Physics, Friedrich-Alexander-Universität Erlangen-Nürnberg, Germany

¹³ DESY, Platanenallee 6, 15738 Zeuthen, Germany

¹⁴ Department of Physics, School of Education, Can Tho University

Campus II, 3/2 Street, Ninh Kieu District, Can Tho City, Vietnam

(Dated: November 29, 2019)

* B.H.Hare@rug.nl

† O.Scholten@rug.nl

I. EMISSION POWER FROM A STREAMER

Here we make an order-of-magnitude estimate of the number of electrons in a streamer from the peak intensity of the observed RF pulses. Since our antennas are very far from the source region, we neglect the inner-structure of the streamer and we take a very simple model for a streamer where a point charge is accelerated and subsequently decelerated [1]. The current moment in the streamer starts at t_1 , and linearly increases until its maximum (of I_0), over an acceleration time of τ . Then the current moment linearly decreases back to 0 at a time t_2 . Therefore, the temporal variation of the current moment can be expressed as

$$\mathbf{I}(t) = \begin{cases} 0 & t \leq t_1 \\ \mathbf{I}_0 \frac{t - t_1}{\tau} & t_1 < t \leq t_1 + \tau \\ \mathbf{I}_0 & t_1 + \tau < t \leq t_2 - \tau \\ \mathbf{I}_0 \frac{t_2 - t}{\tau} & t_2 - \tau < t \leq t_2 \\ 0 & t > t_2 \end{cases} . \quad (1)$$

Since the current moment is due to a point charge we have $\mathbf{I}_0 = Q \mathbf{v}$, where Q is the total charge in the streamer header, \mathbf{v} is peak speed. The electric field is given by the Maxwell equation

$$\mathbf{E}(t) = -\nabla\phi - \frac{d\mathbf{A}}{dt} , \quad (2)$$

where, in the Lorentz Gauge for a point charge at a large distance we have

$$\mathbf{A}(D, t) = \frac{1}{4\pi\varepsilon_0 c^2} \frac{\mathbf{I}(t')}{D} . \quad (3)$$

where D is the large distance from the antenna to the source (retardation effects can be ignored since the motion is non relativistic) and t' is the retarded time. Since we are only sensitive to the radiation component, the $\nabla\phi$ term is negligible. Thus the electric field, at a distance D perpendicular to the direction of current is

$$\mathbf{E}(t) = \begin{cases} 0 & t \leq t_1 \\ \frac{Q \mathbf{v}}{4\pi\varepsilon_0 D \tau c^2} & t_1 < t \leq t_1 + \tau \\ 0 & t_1 + \tau < t \leq t_2 - \tau \\ \frac{-Q \mathbf{v}}{4\pi\varepsilon_0 D \tau c^2} & t_2 - \tau < t \leq t_2 \\ 0 & t > t_2 \end{cases} . \quad (4)$$

This results in a power density in the form of two pulses, each with strength

$$P_s = \frac{\mathbf{E}^2}{Z_0} = \frac{1}{(4\pi)^2 \varepsilon_0 c^3} \left(\frac{Q v}{\tau D} \right)^2 , \quad (5)$$

where $Z_0^{-1} = \varepsilon_0 c$. The total energy in the pulse is now

$$E_{\text{tot}} = 2\tau P_s . \quad (6)$$

To relate the peak power, P_s , to the strength of a pulse we see with LOFAR we have to take into account that the LOFAR frequency window ranges from 30 – 80 MHz, and thus only a fraction F will be received. For a short pulse with a width between 1 – 10 ns, F will be about 0.1. In addition the sources are close to the horizon for which the sensitivity of the LOFAR antennas is reduced. For a zenith angle of 80° this reduction factor is about $A \approx 1/20$ in power.

The amplitude of the signal S will be expressed in units of the amplitude of the background, mostly galactic background. The strongest radio pulses we observe from negative leaders have amplitudes around $S = 200$. In Ref. [2] the noise power of the LOFAR antennas is determined to be about 4×10^{-14} W/MHz over the 30 – 80 MHz band and thus $P_n = 2 \times 10^{-12}$ W. The power in the signal can now be written as $P_s F A = P_n \times S^2$. Putting all factors together we obtain

$$\begin{aligned} Q &= \sqrt{P_s (4\pi)^3 \varepsilon_0 c^3} \frac{\tau D}{v} = S \sqrt{\frac{P_n (4\pi)^2 \varepsilon_0 c^3}{AF}} \frac{\tau D}{v} \\ &= 4(S/100) (\tau/\text{ns}) (D/10\text{km}) (1 \text{ mm ns}^{-1}/v) [\mu\text{C}] \end{aligned} \quad (7)$$

relating the measured pulse amplitude S for an antenna at a distance D to the total charge Q in a streamer and where we have used that the effective area of a LOFAR antenna for radiation from zenith is about 1 m^2 .

For our strongest pulses, which have amplitudes of $S = 200$ recorded on antennas $D = 10 \text{ km}$ from the source, we find that the total charge has an order-of-magnitude around $8 \mu\text{C}$ or 5×10^{13} electrons. This assumes that $\tau = 1 \text{ ns}$, since an order-of-magnitude larger or smaller would cause the pulse to be outside our frequency range, and that $v = 1 \text{ mm/ns}$, based on simulated speeds of negative streamers [3] and measured speeds of positive streamers [4].

It may be of interest to calculate the total energy from our strongest pulses that is radiated in the our frequency band ($30 - 80 \text{ MHz}$)

$$\begin{aligned} E &= 2\tau P_s 4\pi D^2 = \frac{\tau P_n S^2 8\pi D^2}{A} \\ &= (S/100)^2 (\tau/\text{ns}) (D/10\text{km})^2 \times 10^{-6} [\text{J}] . \end{aligned} \quad (8)$$

To put these numbers in perspective a comparison can be made with the streamer modeling as presented in Ref. [3] where the tip of a negative streamer (see their figure 5) contains about 6×10^{10} electrons. In Ref. [5] (fig 6) a complex of streamers from the same stem is shown having a total charge content of many 10's [nC], increasing with time. Ref. [6] used streamers with a diameter of about 3 mm, length of about 0.5 cm, and had an electron density of about 10^{21} m^{-3} , which results in streamers with about 10^{10} electrons. Thus, the streamers we observe are stronger than typical streamers produced by simulations, which is understandable since in simulations the number of electrons in the head of a streamer is strongly related to the voltage and diameter of the emitting electrode [3, 4]. Thus natural streamers could easily have orders-of-magnitude more charge than typical simulated streamers. In addition one should realize than there are about 10^5 or more streamers in a negative leader where we only detect the strongest few [7]. Therefore, it is entirely reasonable that the vast majority of streamers are too weak for us to measure, and that only the strongest are intense enough for use to measure distinct RF pulses.

II. TYPICAL BURSTS

Below are a number of figures that show different bursts on negative leaders. In each of these figures the panels on the left give an overview of the whole local leader section, with the relevant burst highlighted in black. The right panels show an expanded view of the relevant burst.

- [1] B. Neijzen, *Negative Leader Propagation*, Bachelor's thesis, University of Groningen, FSE, KVI-CART (2019).
- [2] K. Mulrey, A. Bonardi, S. Buitink, A. Corstanje, H. Falcke, B. Hare, J. Hrandel, T. Huege, P. Mitra, A. Nelles, J. Rachen, L. Rossetto, P. Schellart, O. Scholten, S. ter Veen, S. Thoudam, T. Trinh, and T. Winchen, Astroparticle Physics **111**, 1 (2019).
- [3] J. Qin and V. P. Pasko, Journal of Physics D: Applied Physics **47**, 435202 (2014).
- [4] T. Briels, J. Kos, E. Veldhuizen, and U. Ebert, J. Phys. D: Appl. Phys. **39**, 5201 (2006).
- [5] A. Luque and U. Ebert, New Journal of Physics **16**, 013039 (2014).
- [6] F. Shi, N. Liu, J. R. Dwyer, and K. M. A. Ihaddadene, Geophysical Research Letters **46**, 443 (2019).
- [7] S. Celestin, W. Xu, and V. P. Pasko, Journal of Geophysical Research : Space Physics **120**, 10712 (2015).

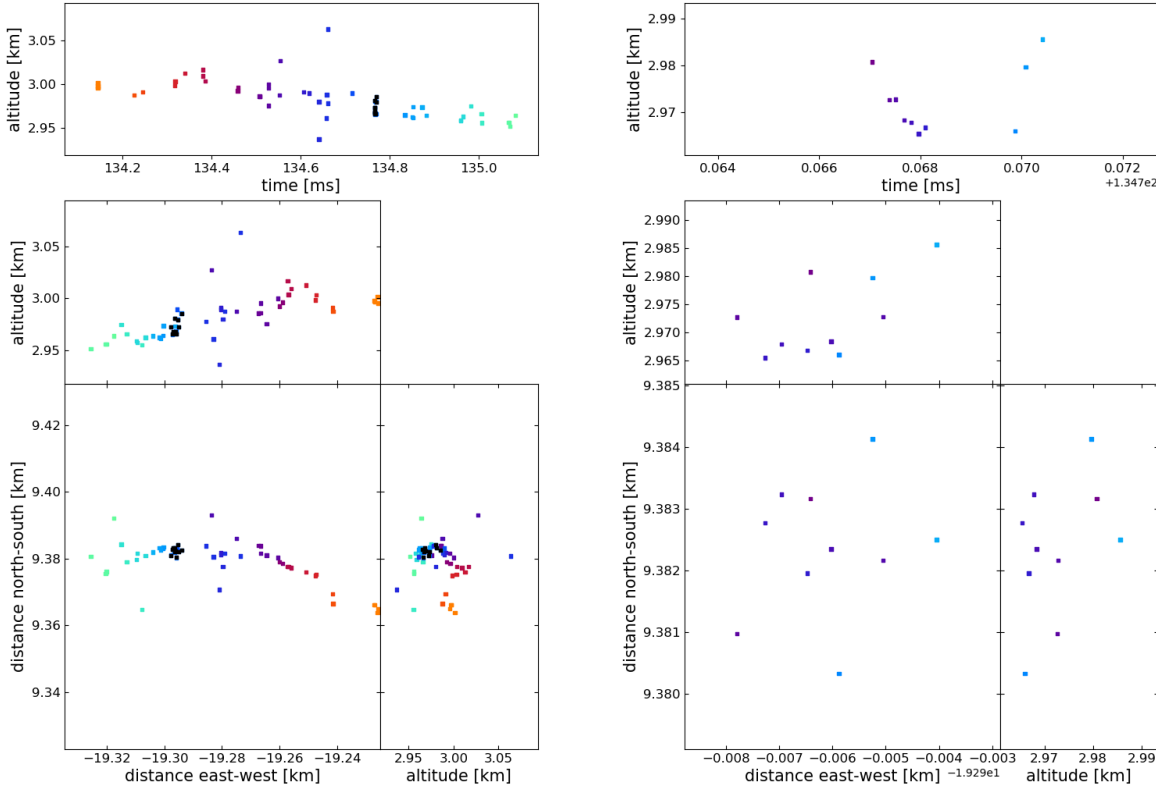


FIG. 1: A burst with a large number of located sources. Left: Overview of the whole leader, which propagates from east to west in the plan view. The sources in the burst are colored black. Right: Zoom-in on the relevant burst.

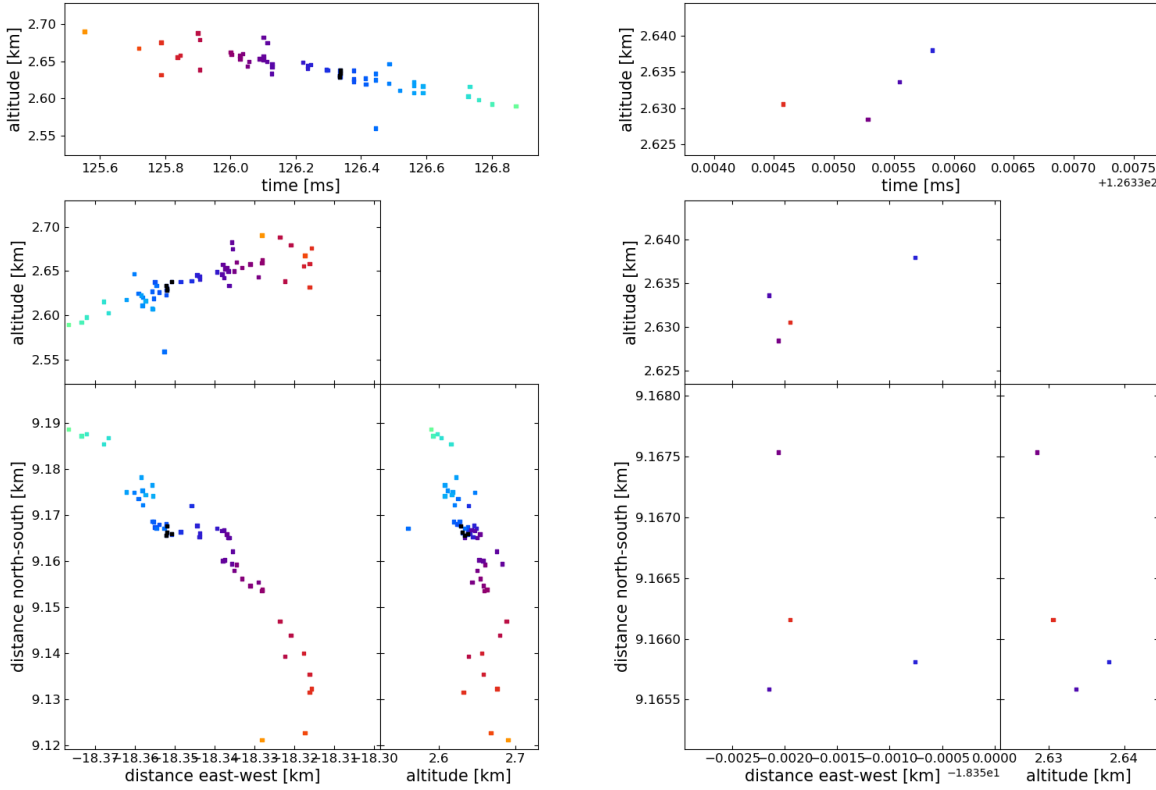


FIG. 2: A burst with four located sources. Left: Overview of the whole leader, which propagates to the north in the plan view. The sources in the burst are colored black. Right: Zoom-in on the relevant burst.

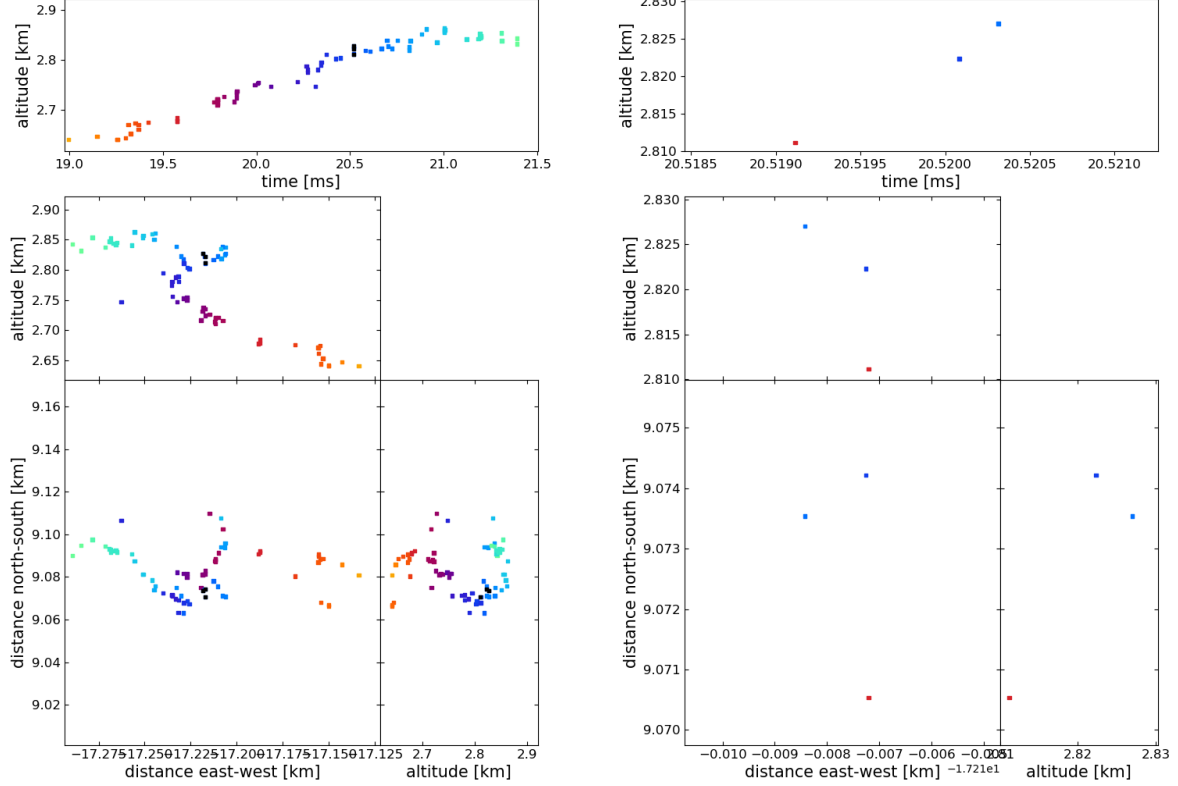


FIG. 3: A burst with three located sources. Left: Overview of the whole leader, which propagates from west to east in the plan view. The sources in the burst are colored black. Right: Zoom-in on the relevant burst.

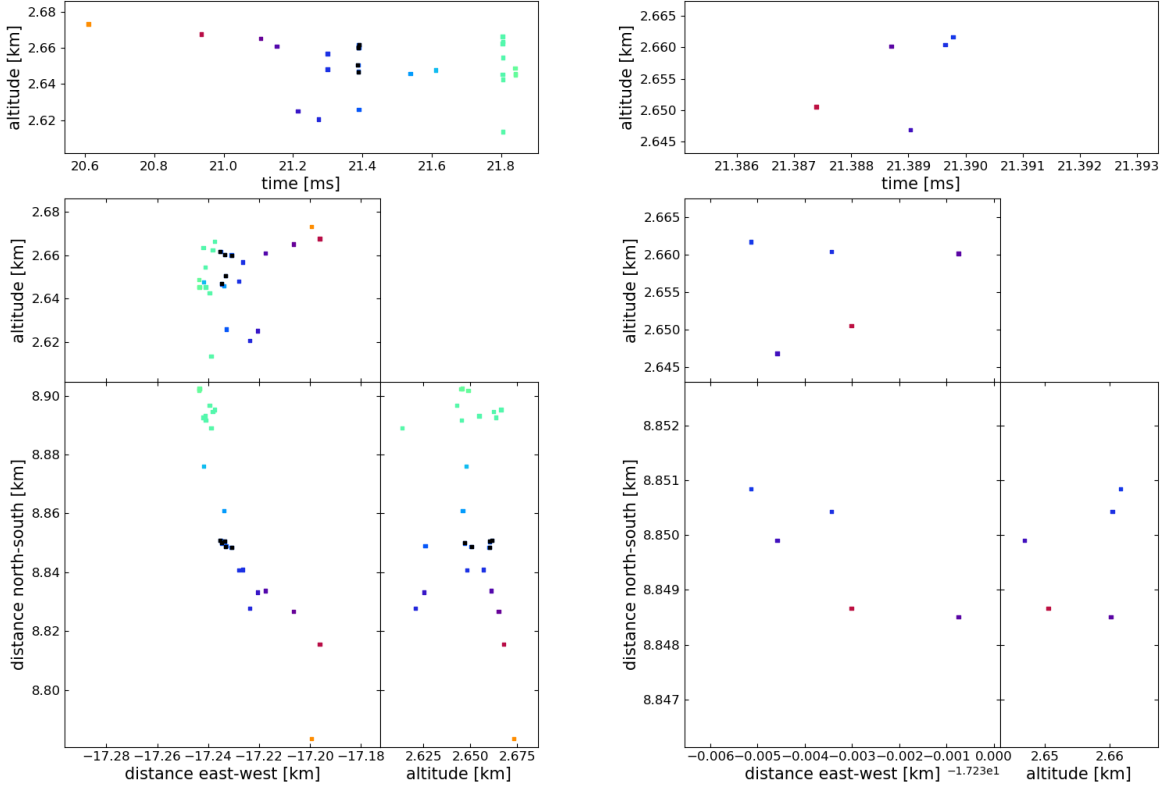


FIG. 4: A burst with five located sources. This burst seems to be more extended in the North-West to South-East direction, which aligns with the direction of the leader. Left: Overview of the whole leader, which propagates to the north in the plan view. The sources in the burst are colored black. Right: Zoom-in on the relevant burst.

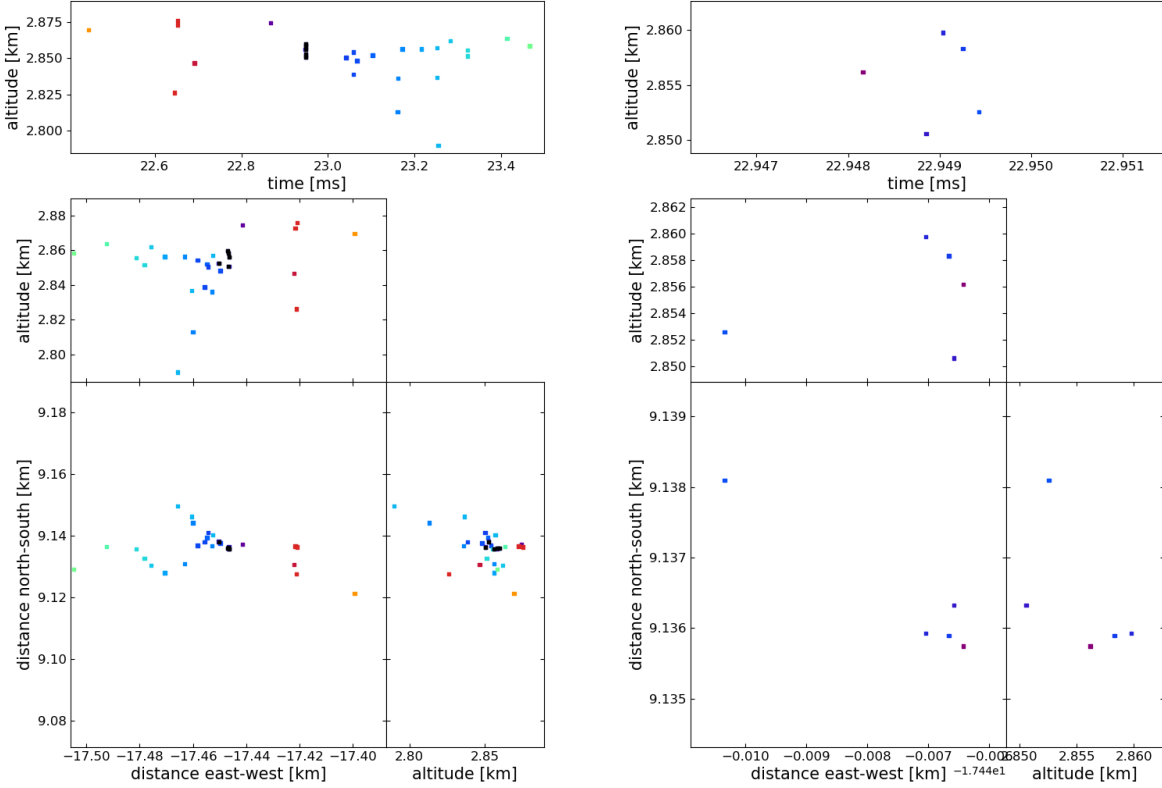


FIG. 5: A burst with five located sources. Four are close together, with one source about four meters away, in the same direction as the leader channel. Left: Overview of the whole leader, which propagates East to West in plan view. The sources in the burst are colored black. Right: Zoom-in on the relevant burst.

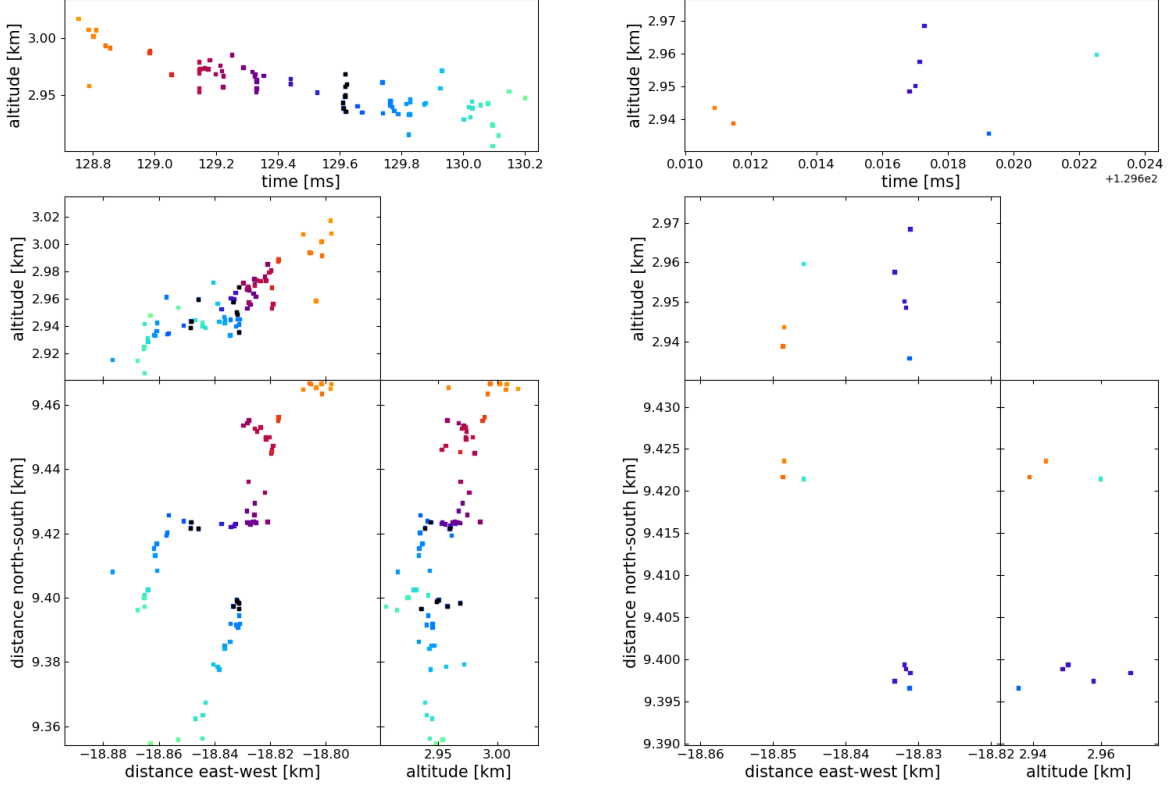


FIG. 6: Two bursts from two leader branches that are very close in time. The leader propagates south, and splits into two branches at about $X=-18.82$ km, $Y=9.42$ km. The west branch ends at about $Y=9.4$ km. The east branch has a distance of about 20 m with no located RF sources, and continues to propagate south. Left: Overview of the whole leader. The sources in the burst are colored black. Right: Zoom-in on the relevant burst.

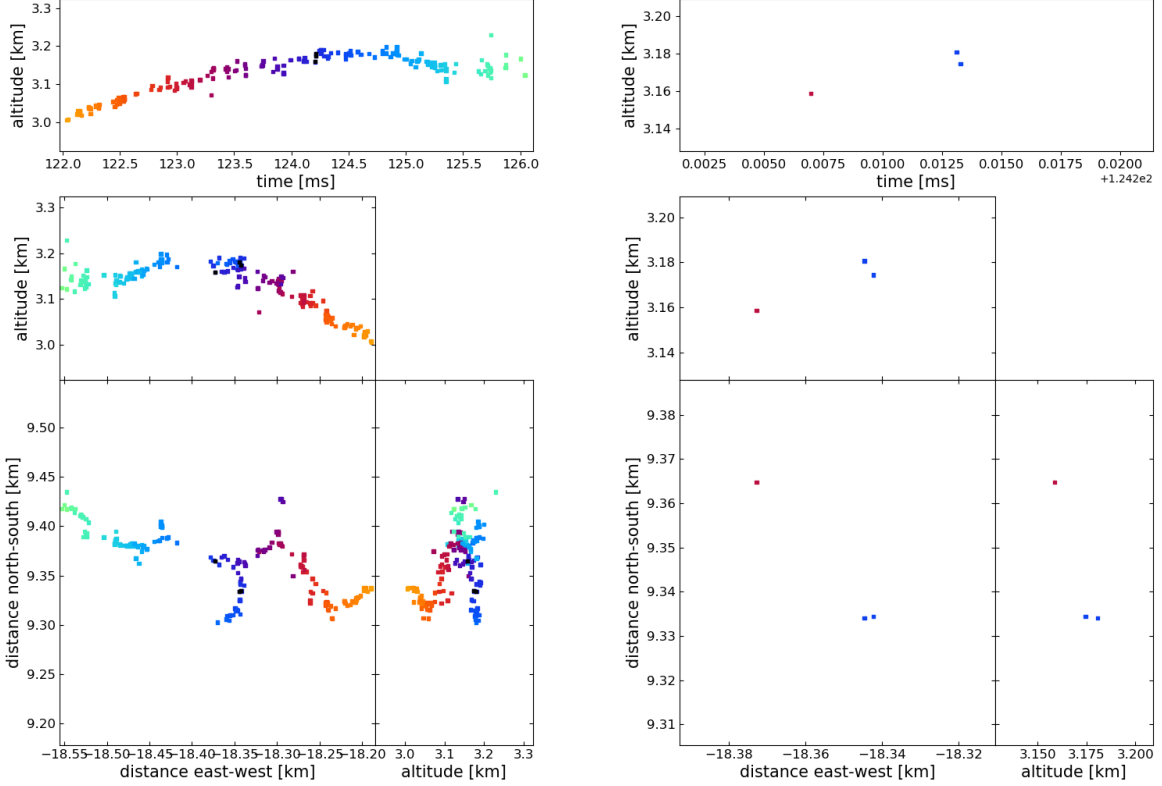


FIG. 7: A leader propagating East to West, with a branch starting at $X=18.35$. The smaller branch propagates south and ceases to propagate after about 75 m. There are two indicated sources on the leader branch, and one on the main channel that are very close in time. Left: Overview of the whole leader. The indicated sources are colored black. Right: Zoom-in on the three sources.